Characterization of Various Oxygen Species on an Oxide Surface: RuO2(110)†

ARTICLE *in* THE JOURNAL OF PHYSICAL CHEMISTRY B · MARCH 2001

Impact Factor: 3.3 · DOI: 10.1021/jp003213j

Characterization of Various Oxygen Species on an Oxide Surface: $RuO_2(110)$†

Y. D. Kim, A. P. Seitsonen,‡ S. Wendt, J. Wang, C. Fan, K. Jacobi, H. Over,* and G. Ertl

Department of Physical Chemistry, Fritz-Haber-Institut der Max-Planck-Gesellschaft, Faradayweg 4-6, D-14195 Berlin, Germany

Received: September 12, 2000; In Final Form: January 18, 2001

The stoichiometric $RuO_2(110)$ surface is terminated by bridge-coordinated oxygen atoms (O_β) and by coordinatively unsaturated Ru (Ru_{cus}) atoms. Exposure to gaseous O_2 leads to the formation of two additional surface species: a molecularly chemisorbed state (O_δ) bridging two neighboring Ru_{cus} atoms and weakly held O atoms (O_γ) in terminal position above the Ru_{cus} atoms. Characterization of the energetics and kinetics as well as structural, vibrational, and electronic properties is achieved by combined application of experimental (low-energy electron diffraction, high-resolution electron loss spectroscopy, thermal desorption spectroscopy) and theoretical (density functional theory) methods. The interplay between the different oxygen species accounts for the high sticking coefficient for dissociative adsorption as well as for the continuous restoration of the surface structure in the course of catalytic oxidation reactions.

1. Introduction

The bond strength and the charge state of oxygen species on the catalyst's surface are considered to govern the activity and selectivity of an oxidation catalyst. This makes a rich oxygen chemistry a necessary prerequisite for a versatile oxidation catalyst.[1] Silver, for instance, is able to stabilize at least five different oxygen species at the surface, i.e., the molecular adsorption state, a chemisorbed atomic species, a dissolved O species, an embedded O species, and the oxidic O species. These O species reveal distinct chemical properties. For the methanol dehydrogenation reaction to formaldehyde over Ag, the strongly held embedded O species in the presence of dissolved O is important,[2] while the chemisorbed species[3] is suggested to determine the selectivity of the epoxidation reaction of ethylene.

Several oxygen species have also been reported for ruthenium: the virtually inactive chemisorbed atomic O species,[4] an oxidic species in the oxygen-rich phases,[5] and a weakly held oxygen adsorbed on the oxygen-rich phase.[6] The latter two species are quite active in the CO oxidation reaction.[6,7] Low-energy electron diffraction (LEED) and scanning tunneling microscopy (STM) investigations showed that the oxygen-rich phases on Ru(0001) consist of both (1×1)-O and $RuO_2(110)$ patches.[5,8] The catalytically active parts of the oxygen-rich phase on Ru(0001) were identified with the (110) rutile face of RuO_2,[5,9] whose active centers are the coordinatively unsaturated Ru sites (Ru_{cus} atoms). The $RuO_2(110)$ surface is terminated by undercoordinated bridging oxygen atoms (O_{br}). Structural defects on the oxide surface do not play a significant role for the activity of RuO_2, quite in contrast to the general view of active centers on oxide surfaces.[10] Oxygen postexposure to the oxygen-rich phase at room temperature creates a weakly bound oxygen species with a dissociative sticking probability of 0.7. This O species desorbs at 450−500 K, and it efficiently catalyzes the CO oxidation even at room temperature.[6]

In this paper we review the various oxygen species on the $RuO_2(110)$ surface in comparison with those on Ru(0001) and present new data by applying the techniques of LEED, high-resolution electron loss spectroscopy (HREELS), and density functional theory (DFT) calculations. Our combined study gives strong evidence that the weakly held oxygen species are adsorbed oxygen atoms which are located in terminal position above the coordinatively unsaturated Ru sites (Ru_{cus}) on $RuO_2(110)$. The vibrational characteristics of the $RuO_2(110)$ surface were studied by HREELS: two dominating losses at 69 and 103 meV are assigned to bridging O and on-top O, respectively. Furthermore our DFT calculations predict a chemisorbed molecular oxygen species which lies down on the $RuO_2(110)$ surface, bridging neighboring Ru_{cus} atoms. The presence of this O_2 species is confirmed by thermal desorption spectroscopy and HREELS. The molecular oxygen species on $RuO_2(110)$ is considered to play a decisive role in the high dissociation probability of O_2 over $RuO_2(110)$.

2. Experimental and Theoretical Details

The LEED experiments were conducted in an ultrahigh vacuum chamber equipped with four-grid LEED optics, thermal desorption spectroscopy (TDS), and facilities for surface cleaning and characterization.[11] The LEED intensity data were recorded at a sample temperature of 110 K, using a computerized, high-sensitivity CCD camera system. The analysis of the experimental LEED data used a multiple scattering program code that allows for the simultaneous and automated refinement of structural (and nonstructural) parameters.[12,13] The agreement between calculated and experimental data was quantified by Pendry's reliability factor R_P.[14]

The HREELS measurements were performed in a second ultrahigh vacuum apparatus, which consists of two chambers. The upper chamber contains an argon ion gun, a quadrupole mass spectrometer, and a LEED optics. The lower chamber houses an HREELS spectrometer for recording the vibrational spectra. The HREEL spectra were all taken at a 60° angle of

† Dedicated to Professor J. T. Yates on the occasion of his 65th birthday. Part of the special issue "John T. Yates, Jr. Festschrift".

* Corresponding author. Fax: +49−30−8413−5106. E-mail address: over@fhi-berlin.mpg.de. URL: http://w3.rz-berlin.mpg.de/pc/pc.html.

‡ Also at INFM, Unità di Roma, Dipto. di Fisica, Università La Sapienza, P.'le A. Moro 2, I-00185 Roma, Italy, and IPP Garching, Boltzmannstr. 2, D-85748 Garching, Germany.

10.1021/jp003213j CCC: $20.00
Published on Web 03/29/2001

incidence with respect to the surface normal and in specular geometry. The sample temperature was 83 K. The energy resolution was set to be 2.7 meV, which ensures a typical counting rate of 3×10^5 counts/s in the elastic peak.

For the DFT calculations we employed the generalized gradient approximation of Perdew et al.[15] for the exchange-correlation functional and used ab initio pseudopotentials in the fully separable form.[16] The surface was modeled by five double layers of RuO_2(110) (supercell approach). Consecutive RuO_2(110) slabs were separated by a vacuum region of about 16 Å. Calculations were performed using a (1×1) surface unit cell. Further details can be found in ref 7. To compute the vibrational frequencies, the position of the respective atom (consistent with the vibrational mode to be studied) was varied symmetrically around its equilibrium position, keeping all other atoms fixed at their equilibrium positions. The corresponding data points (in general five including the equilibrium position) were fitted to a parabolic function from which the vibrational frequency was derived.

In both chambers (HREELS and LEED), the Ru(0001) sample was cleaned by argon ion bombardment at 1 keV followed by cycles of oxygen adsorption and thermal desorption in order to remove surface carbon. Final traces of oxygen were removed by flashing the surface to 1530 K, resulting in a sharp (1×1) LEED pattern. No impurity losses were observed in HREELS.

The oxygen-rich ruthenium phase for the LEED experiments was produced by exposing a well-prepared single-crystal Ru(0001) to high doses of oxygen at an elevated sample temperature of 600 K. To reduce the oxygen background pressure in the ultrahigh vacuum chamber, oxygen was dosed through a glass capillary array doser (with channels 3 mm long and 10 μm wide, total transparency of 50%) about 1 mm away from the sample. In this way, the local oxygen pressure at the sample could be enhanced by a factor of about 100, thus allowing the oxygen partial pressure in the ultrahigh vacuum chamber to be kept below 10^{-5} mbar during dosing. Typical oxygen exposures (local pressure $\times$ time) for the preparation were 6×10^6 langmuirs. After the background pressure in the ultrahigh vacuum chamber has reached a value below 10^{-9} mbar, the sample was briefly annealed to 600 K in order to remove contamination by residual gas adsorption. The sample was then cooled to 100 K. The total amount of oxygen in the oxygen-rich Ru(0001) surface used in the LEED experiment was equivalent to about 6 monolayers, as estimated by a thermal desorption experiment. The corresponding LEED pattern indicates that the surface consists of patches of both Ru(0001)−(1×1)-O and RuO_2(110).

The oxygen-rich Ru(0001) surface for the HREELS measurements was produced by exposing 1×10^7 langmuirs of O_2 at 700 K. The glass capillary array doser was about 15 mm away from the sample, yielding an enhancement of about 30. This procedure resulted in a surface, which was completely covered by RuO_2(110), as checked by LEED and HREELS.

The weakly held oxygen (O_γ) was produced by exposing several langmuirs of O_2 (for instance 5 langmuirs) to RuO_2(110) at room temperature, while the molecular oxygen (O_δ) was prepared by exposing O_2 to the sample at 100 K. Note that O overlayers on Ru(0001) are not able to stabilize a O_2 species above 40 K. For the definition of the various O species on Ru(0001) and RuO_2(110) we refer to the TD spectrum in Figure 1. The desorption state of the chemisorbed atomic oxygen species on Ru(0001) is indicated by (O_α), while the oxidic oxygen of RuO_2(110) is denoted as (O_β).

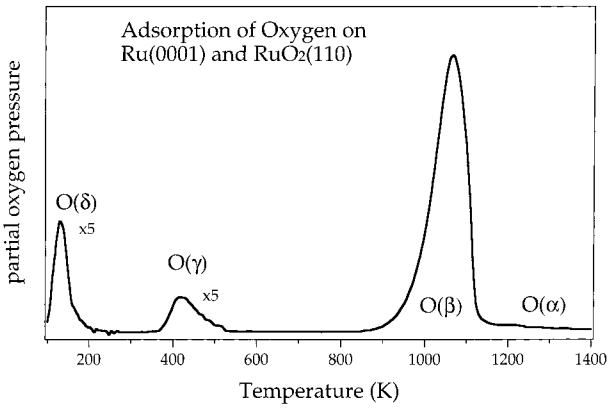

Figure 1. Thermal desorption spectra of oxygen on Ru(0001) and RuO_2(110). The desorption states O_α, O_β, O_γ, and O_δ correspond to chemisorbed oxygen on Ru(0001), lattice oxygen of RuO_2(110), weakly held oxygen on RuO_2(110), and molecular oxygen on RuO_2(110), respectively. The spectra of O_γ and O_δ are amplified by a factor of 5.

3. Results and Discussion

3.1. Surface Structure. Chemisorbed oxygen is able to form four ordered overlayer phases on Ru(0001), i.e., (2×2)-O, (2×1)-O, (2×2)-3O, and (1×1)-O. In all cases the oxygen atoms occupy hcp 3-fold hollow sites with the O−Ru bond length decreasing from 2.03 to 2.00 Å with increasing coverage.[4] Increasing the O coverage beyond 2−3 monolayers leads to the epitaxial growth of RuO_2(110) on Ru(0001) which may coexist with (1×1)-O on Ru(0001), depending on the sample temperature during preparation. By using NO_2 instead of O_2, O-rich phases with O contents of up to the equivalent of 5 monolayers on Ru(0001) can be produced without oxidizing the sample.[9,17] These surface structures are characterized by a (1×1)-O overlayer and several monolayers of oxygen incorporated in the near-surface region.[9]

The as-grown RuO_2(110) surface is terminated by a bridging oxygen atom O_{br}.[8] In the bulk structure of RuO_2 the Ru atoms are 6-fold coordinated to oxygen atoms, while the O atoms are coordinated to three Ru atoms in a planar sp^2 hybridization. On the RuO_2(110) surface two kinds of undercoordinated surface atoms are present, namely, the bridging oxygen atoms, which are coordinated only to two Ru atoms underneath (bond length: 1.94 Å), and the so-called Ru_{cus} atoms, i.e., 5-fold coordinated Ru atoms.[8] The other Ru−O bond lengths are in the range of 1.90−2.03 Å. Noteworthy, DFT and LEED gave practically identical structural parameters for the RuO_2(110) surface.

To study the structural characteristics of the weakly held oxygen (O_γ), we monitored the intensity variation of LEED beams associated with the (1×1)-O and RuO_2(110) phases during postdosing oxygen at room temperature. O_2 exposure at room temperature does not change the appearance of the LEED pattern, and only the RuO_2(110) related LEED intensities were affected. This implies that the weakly held oxygen atoms O_γ adsorb only on the oxide domains rather than on the (1×1)-O areas. Besides the absolute intensity change on O_2 exposure, also the structure of the LEED IV curves altered. We therefore conclude on a specific (i.e., well-defined) adsorption site of O_γ. A detailed LEED analysis of O_γ−RuO_2(110) related LEED IV curves disclosed the adsorption site of O_γ to be directly above the Ru_{cus} atom (cf. Figure 2) with an O−Ru bond distance of 1.85 Å. The agreement between experimental and calculated LEED IV curves for the optimized model structure of O_γ−RuO_2(110) is quantified by $R_P = 0.35$ (cf. Figure 3). The LEED analysis yields that $75 \pm 20\%$ of the Ru_{cus} atoms are occupied

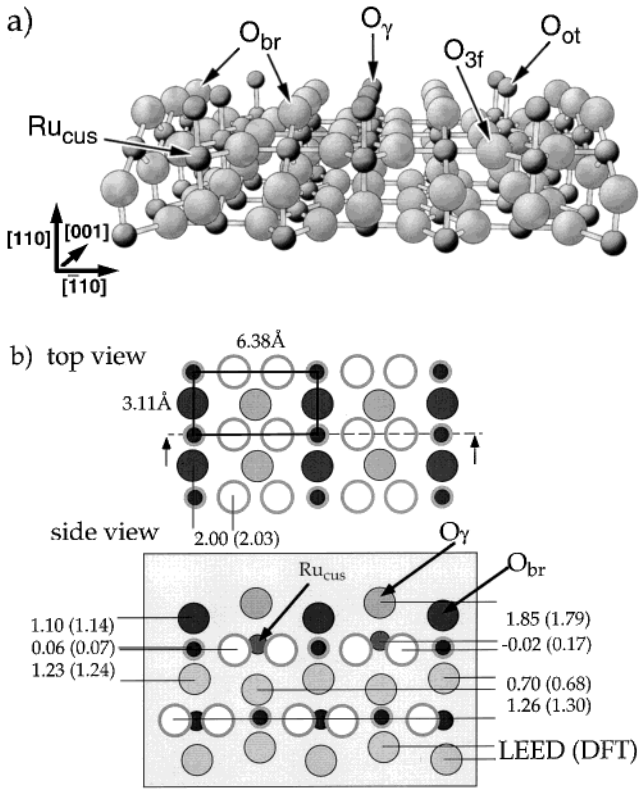

Figure 2. (a) Stick and ball model of the $O_\gamma-RuO_2(110)$ surface. Large balls represent oxygen, and small balls represent ruthenium atoms of $RuO_2(110)$. A bridge-bonded (O_{br}), an on-top bonded (O_γ), and a 3-fold coordinated O atom are indicated. (b) The optimum surface geometry of the $O_\gamma-RuO_2(110)$ as determined by LEED and DFT calculations. All values are given in angstroms. The corresponding layer spacings in bulk RuO_2 are 1.27 and 0.635 Å. The $O_\gamma-Ru$ bond length is 1.85 Å.

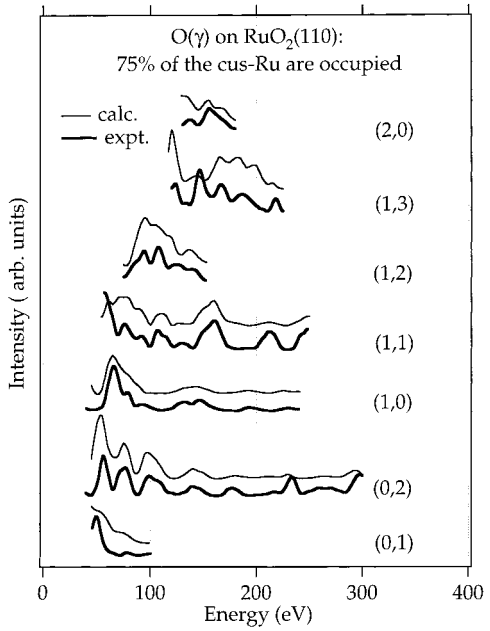

Figure 3. Comparison between experimental and calculated LEED IV curves for the optimum surface structure of the weakly held oxygen O_γ on $RuO_2(110)$. The agreement is quantified by $R_P = 0.35$.

by O_γ. Thereby, the underlying $RuO_2(110)$ surface undergoes only minor structural changes upon O adsorption. Most notably, however, the Ru_{cus} atoms move outward by 0.1 Å when capped by O_γ, to establish a bulklike environment. The adsorption of

TABLE 1: Calculated DFT Binding Energies for the Systems O−Ru(0001) and $RuO_2(110)$[a]

O species	binding energy (eV)	O species	binding energy (eV)
Ru(0001)−(2×2)-O hcp	5.87	Ru(0001)−(1×1)-O hcp	5.07
Ru(0001)−(2×1)-O bridge	4.82	O(bridge)−RuO_2(110)	4.60
Ru(0001)−(2×2)-O top	4.23	O(3-fold)−RuO_2(110)	5.80
Ru(0001)−(2×1)-O hcp	5.52	O(on-top)−RuO_2(110)	3.20
Ru(0001)−(2×2)3O hcp	5.29	O_2−RuO_2(110)	0.80

[a] The internal O−O binding energy of O_2 is calculated to be 6.0 eV. Except for the moelcular oxygen, all other energies are given with respect to atomic oxygen.

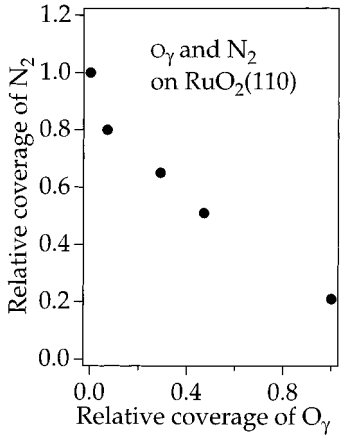

Figure 4. $RuO_2(110)$ surface precovered by various coverages of O_γ and subsequently saturated by N_2. N_2 is known to adsorb directly above the Ru_{cus} atoms. If O_γ occupy the same adsorption site as N_2, then the coverages of O_γ and N_2 are related by $\theta(O_\gamma) = \theta(Ru_{cus}) - \theta(N_2)$. $\theta(Ru_{cus})$ is the number of cus atoms on $RuO_2(110)$.

O_γ transforms the Ru_{cus} atom into a bulklike (i.e., 6-fold coordinated) Ru atom, as also corroborated by recent high-resolution surface core level shift (SCLS) measurements.[18] Similar structural results were also obtained by DFT calculations. The $Ru-O_\gamma$ bond length turned out to be 1.79 Å, which is markedly shorter than the O−Ru bond length of chemisorbed atomic oxygen on Ru(0001) (2.00−2.03 Å)[4] and in $RuO_2(110)$ (1.93 and 2.00 Å).[8] This result is quite remarkable and may point to a coordination effect, since the binding energy of $O_\gamma-Ru_{cus}$ is only 3.2 eV according to our DFT calculations and therefore significantly lower than that of the bridging $O_\gamma-Ru$ bonding of 4.6 eV (cf. Table 1). The low adsorption energy makes O_γ a potentially active species.

The adsorption site of O_γ can also be titrated by coadsorbing N_2 onto $RuO_2(110)$. The basic property which allows this kind of titration experiment is that N_2 adsorb above the Ru_{cus} atoms with their molecular axes normal to the surface plane.[19] Therefore, O_γ and N_2 will compete for the same adsorption sites, if O_γ adsorbs over Ru_{cus} atoms. In the N_2 titration experiments, the $RuO_2(110)$ surface is precovered with various coverages of O_γ, and subsequently, the surface is saturated by N_2. In the saturated $N_2-RuO_2(110)$ overlayer all Ru_{cus} atoms are capped.[19] With TDS both of the relative coverages of O_γ and N_2 were measured. The titration experiments[19] indicate that, with increasing O_γ coverage, the N_2 coverage decreases in a way in which the total coverage of N_2 and O_γ is preserved (cf. Figure 4). This finding provides additional evidence for the on-top adsorption of O_γ. At saturation of O_γ, still some N_2 (20% of its saturation coverage) can adsorb on $RuO_2(110)$. This supports the above LEED analysis which indicates that only 75% of Ru_{cus} atoms are capped by O_γ at saturation.

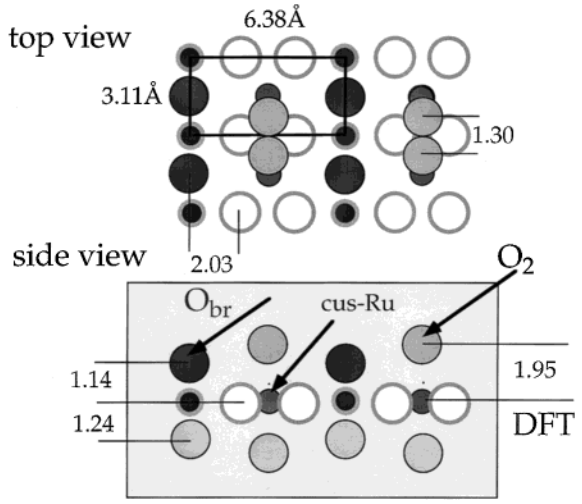

Figure 5. Optimum surface geometry of the $O_2-RuO_2(110)$ as determined by DFT calculations. O_2 bridges two neighboring Ru_{cus} atoms. All values are given in angstroms. The internal O−O bond length is 1.30 Å, while the O−Ru bond length is 2.16 Å.

The DFT calculations predicted a molecular oxygen species O_δ on $RuO_2(110)$. The local adsorption geometry is defined by a flat lying oxygen molecule, which bridges two neighboring Ru_{cus} atoms (cf. Figure 5). The internal O−O bond length of this species is 1.30 Å, and the O−Ru bond length is 2.16 Å; note that the O−O bond length in a free O_2 molecule is calculated to be 1.22 Å. In comparison to O_2 on Pt(111),[20,21] the structural properties of O_2 on $RuO_2(110)$ are compatible with a superoxo-like O_2^- species. DFT calculations of O_2 on Pt(111) revealed 1.34 Å for the O−O bond length and 2.07 Å for the Pt−O bond length.[22]

3.2. Energetics. Oxygen atoms chemisorbed on Ru(0001) (O_α) form various ordered phases and desorb associatively between 1100 and 1700 K on heating the sample (cf. Figure 1). The heat of adsorption was roughly estimated to be 400 kJ/mol (low coverage value) and 315 kJ/mol (0.5 monolayer), assuming second-order desorption.[23] More recent values for the heat of adsorption as a function of O coverage were provided by a combined TDS/DFT investigation: 4.9 eV (very low O coverage), 4.25 eV (0.25 monolayer), 3.5 eV (0.5 monolayer), 3.0 eV (0.75 and 1.0 monolayer).[24] At O coverages of 0.25, 0.5, 0.75, and 1 monolayer (2×2)-O, (2×1)-O, (2×2)-3O, and (1×1)-O overlayers are formed, respectively. Beyond an oxygen coverage of 1 monolayer, O_2 desorption takes place at 1040 K; the corresponding desorption state is referred to as (O_β) in Figure 1. As previously shown,[5,8] excessive oxygen exposure to Ru(0001) at sample temperatures of 600−800 K leads to the epitaxial growth of ultrathin $RuO_2(110)$ domains, which may coexist with the (1×1)-O phase. Decomposition of this phase is accompanied by O_2 desorption with a TDS peak at 1040 K (O_β state). The bond strength of O_β is thus considerably lower than for O atoms chemisorbed on Ru(0001) (O_α). From TDS the bridging O species cannot be differentiated from the 3-fold coordinated lattice O of $RuO_2(110)$.

The calculated binding energies (DFT) of oxygen on Ru(0001) as a function of the coverage are collected in Table 1 together with the bond strengths for the various oxygen species on $RuO_2(110)$. All DFT calculations were performed with the same program and the same pseudopotentials to ensure comparability. Clearly, the O−Ru bond strength of the O/Ru(0001) phases decreases by 0.8 eV when the coverage is increased from 0.25 to 1.0 monolayer; an identical trend was reported in a previous DFT study.[25] The bridging O species of $RuO_2(110)$ is even more weakly bound by 0.5 eV than O in Ru(0001)−(1×1)-O. The 3-fold coordinated lattice O atoms of $RuO_2(110)$ reveal a binding energy which is close to that of the (2×2)-O. However, if the bridging oxygen atoms are removed from the surface, then the thus generated 4-fold coordinated Ru atoms agglomerate in Ru clusters, thereby destabilizing the former 3-fold coordinated surface O atoms. This may explain why no extra desorption state is resolved in TDS for bridging O and 3-fold coordinated O on $RuO_2(110)$. It is quite interesting to note that O in the bridging position on the Ru(0001) surface, which is considered to be the transition state for the CO oxidation over Ru(0001),[26] reveals a binding energy which is similar to that of O_{br} on $RuO_2(110)$ (cf. Table 1).

TABLE 2: Vibrational Losses of O Chemisorbed on Ru(0001) and in $RuO_2(110)$[a]

O species	HREELS: vibration (meV)	ref	DFT: vibration (meV)
low-coverage O	perp = 54	30	
Ru(0001)−(2×2)-O	perp = 64	44	67.1
Ru(0001)−(2×1)-O	perp = 73, lat = 53	38	
Ru(0001)−(2×2)3O	perp = 80, lat = 67	38	
Ru(0001)−(1×1)-O	perp = 81	30	80.2
O(bridge)−$RuO_2(110)$	perp = 69	this work	perp = 63
O(on-top)−$RuO_2(110)$	perp = 103	this work	perp = 99
$O_2-RuO_2(110)$	O−O = 142	this work	O−O = 134

[a] "Perp" and "lat" stand for the perpendicular and the lateral vibrations of oxygen, respectively.

Exposing the $RuO_2(110)$ surface to oxygen at room temperature leads to the population of a weakly held oxygen species (Figure 1, desorption state: O_γ) which desorbs in the temperature range of 400−500 K with second-order kinetics.[6] Saturation of this desorption state occurs at an oxygen exposure of 5−10 L. The O_γ-Ru_{cus} binding energy is 3.2 eV and is therefore significantly lower than the bridging oxygen (cf. Table 1). It may be interesting to compare O_γ with the on-top O species identified on MoO_3 [27] and V_2O_5.[28] Cluster calculations have shown that the bond strength (7.64 eV, 7.09 eV) of the on-top O species on MoO_3 is higher than that of the highly coordinated O atoms (6.81 eV).[27] Therefore, this O species is not considered to be particularly important for the activity of MoO_3.[29]

In Table 1 we compare the binding energy of the chemisorbed oxygen atoms on Ru(0001) dependent on the coverage and the coordination number. Clearly, by going from the 3-fold hollow (hcp) to the bridge and finally to the on-top position, the adsorption energy changes by 0.8 and 1.6 eV, respectively. We may therefore conclude that the lower binding energy of the bridging O and the on-top O on $RuO_2(110)$ is mainly a consequence of the lower coordination.

The molecular species O_δ on $RuO_2(110)$ was experimentally identified by a desorption state at about 140 K (cf. Figure 1). O_2 on $RuO_2(110)$ is bound by 0.8 eV as estimated by our DFT calculations, thus being comparable in bond strength with O_2 on Pt(111).[21,22]

3.3. Vibrations. For very low coverages of chemisorbed oxygen on Ru(0001), a vibrational loss at 54 meV is observed in HREELS, which was assigned to the perpendicular O against Ru vibration.[30] With increasing O coverage, this stretching mode then shifts from 61 meV for the (2×2)-O to 81 meV for the (1×1)-O (cf. Table 2 for particular values). In Figure 6, we present HREEL spectra of the as-grown $RuO_2(110)$ surface in comparison with the O_γ covered $RuO_2(110)$ surface and the Ru(0001)−(1×1)-O. In the $RuO_2(110)$ related spectra, no loss at 81 meV is discernible, consistent with a complete $RuO_2(110)$ film covering the Ru(0001) surface. The oxide spectra are not

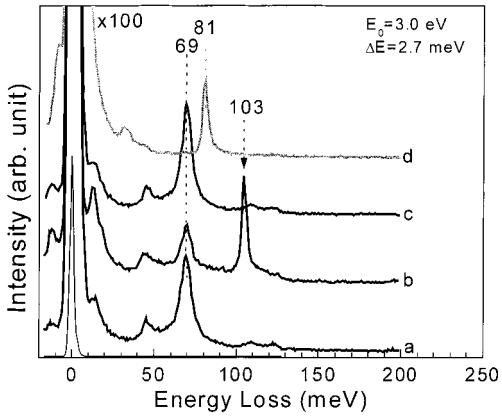

Figure 6. High-resolution electron loss spectra for the clean RuO_2-(110) surface (a) and $O_\gamma-RuO_2$(110) (b). The clean spectrum is dominated by a vibrational loss (69 meV) due to O_{br} against Ru. The additional loss at 103 meV in the $O_\gamma-RuO_2$(110) is assigned to atomic oxygen in the terminal position above Ru_{cus}. Both assignments are based on DFT calculations. (c) $O_\gamma-RuO_2$(110) after heating to 550 K in order to remove O_γ. (d) For comparison the vibrational spectrum of Ru(0001)−(1×1)-O is taken from ref 31. All spectra are recorded in specular geometry with a primary energy of 2.5 eV. The scaling factor in the loss region is 100.

disturbed by the appearance of strong Fuchs−Kliewer phonons due to the metallic character of RuO_2(110). The clean RuO_2(110) surface is dominated by a vibrational loss at 69 meV, which we attribute to the stretching mode of O_{br} against the Ru atoms underneath. This assignment is based on our DFT calculations that determined the $O_{br}-Ru$ stretching mode on the clean RuO_2(110) surface to be 63 meV in nice agreement with the experimental value. Other (but less strong) vibrational losses in Figure 6 are at 108 and 123 meV; the nature of these vibrational modes are unclear. The vibrational loss at 45 meV is in the range of vibrations, which were ascribed to RuO_2 on the basis of surface enhanced Raman scattering (SERS) and Raman spectroscopy.[31,32] It is important to recall that those investigations are performed under electrochemical conditions where the degree of order and crystallinity, in particular the exposed surface plane of RuO_2, were largely unknown. In this context, we emphasize that under electrochemical conditions nanoclusters of RuO_2(100) are grown on Ru(0001),[33] while under ultrahigh vacuum conditions large areas of RuO_2(110) are formed. This uncertainty may account for some of the deviations in the vibrational spectra obtained by SERS/Raman and HREELS. It is also worthwhile to mention that SERS and Raman investigations identified a vibrational loss at about 80 meV with RuO_2(110).[31,32] As evidenced by HREELS (cf. Figure 6), this vibrational mode is not associated with RuO_2(110), but rather with the (1×1)-O overlayer, which may coexist with the oxide.

If compared with the clean RuO_2(110) surface, the O_γ covered RuO_2(110) surface (cf. Figure 6) exhibits an additional loss at 103 meV in the HREEL spectrum, which is therefore related to O_γ. Flashing the O_γ covered RuO_2(110) surface to 550 K removed the weakly held oxygen, as known from TDS, but also seen in HREELS (Figure 6, spectrum c). DFT calculations with supercell geometry determined for O_γ in on-top configuration an O-against-Ru stretching mode at 99 meV, which again compares favorably with the experimental value of 103 meV. In the literature[31,32] this vibrational mode was erroneously assigned to RuO_3. On the $O_\gamma-RuO_2$(110) surface, the intensity of the O_{br}-against-Ru stretching mode is markedly reduced in comparison with the clean RuO_2(110) surface (cf. Figure 6, spectra a + b). Since the O_γ atoms in on-top position stick further out of the surface by about 0.7 Å than the O_{br} atoms, O_γ may screen the $O_{br}-Ru$ vibration mode.

TABLE 3: Work Function of Oxygen on Ru(0001) and RuO_2(110) As Determined by DFT Calculations and Experiments[a]

	work function (eV)		
system	DFT	expt	ref
Ru(0001)	5.03	5.37	46
Ru(0001)−(2×2)-O	5.42	5.65	6
Ru(0001)−(2×1)-O	6.07	6.0	6
Ru(0001)−(2×2)-3O	6.54	6.4	6
Ru(0001)−(1×1)-O	6.74	6.7	6
RuO_2(110)	5.90	5.8[b]	6
RuO_2(110)−(1×1)-O_γ	7.40[a]	6.6[b]	6
O_2-RuO_2(110)	6.75		

[a] The experimental coverage was only 75% of RuO_2(110)−(1×1)-O_γ. [b] The Ru(0001) surface was not completely covered by RuO_2(110).

The molecular oxygen species O_δ reveals a vibrational loss at 142 meV, which is assigned to the internal O−O stretching mode based on our DFT calculations (with a value of 134 meV).

3.4. Electronic Properties. According to our DFT calculations, the work function of the chemisorbed species O_α on Ru(0001) increases from 5.03 to 6.74 eV when increasing the coverage from 0.25 to 1.0 monolayer (cf. Table 3). These values agree nicely with the experimental ones. The DFT calculated work function of the RuO_2(110) surface is 5.9 eV, which rises to 7.40 eV when the surface is saturated by O_γ. Experimentally, the work function for a 6 monolayers precovered O-rich Ru(0001) phase is 5.8 eV and increases to 6.6 eV when the surface was saturated by O_γ.[6] The deviation in the work function change between experiment and theory may be traced to the fact that the Ru(0001) surface was not completely covered with RuO_2(110) in the experiments and that the saturation coverage of O_γ is 75% rather than 100% of the Ru_{cus} atoms as assumed in our DFT calculations. The strong increase in the work function with the population of O_γ is compatible with the on-top adsorption of O_γ, since the dipole length is large and the O_γ atom is strongly polarized as indicated by our DFT calculations (cf. Figure 7).

In the literature of oxide surface chemistry nucleophilic and electrophilic oxygen atoms have been introduced to account for the activity and selectivity of particular reactions, such as the partial oxidation of methanol to formaldehyde or the ethylene epoxidation reaction. For the latter reaction, the concept of electrophilic oxygen (electron accepting, oxygen in a lower valence state) was introduced for Ag catalysts.[3,34] To allow for a close approach of O to the C=C double bond, the electron cloud of electrophilic oxygen should be contracted. Actually, this requirement is met with the weakly held oxygen O_γ on RuO_2(110) (cf. Figure 7). Density difference plots obtained by DFT calculations indicate that the charge cloud around O_γ is indeed more contracted than for O_{br}. O_γ on RuO_2(110) may therefore represent a promising candidate for an electrophilic O species.

At this point, a critical comment about electrophilic and nucleophilic oxygen has to be made. These concepts are adopted from molecular chemistry. In an oversimplified view, nucleophilic oxygen is identified with O^{2-} and electrophilic oxygen with $O^{-\epsilon}$ ($e < 2$). However, a direct correspondence to the charge state and electron distribution of oxygen is certainly not appropriate as exemplified with RuO_2. Our DFT calculations estimated the charge transfer from Ru to oxygen in RuO_2 to be only 0.3e so that none of the oxygen atoms in RuO_2(110) would be nucleophilic in a strict sense.[35] In contrast, a charge state of

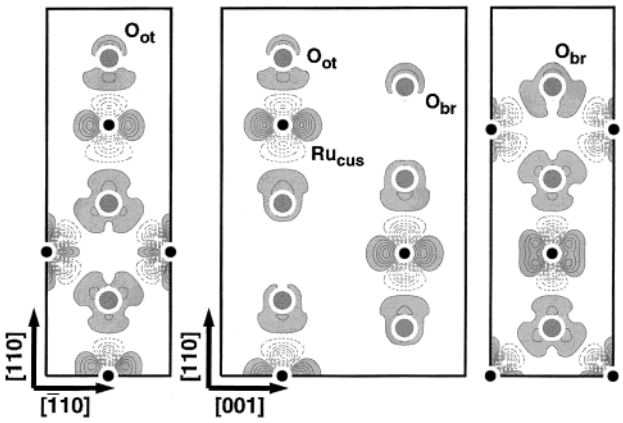

Figure 7. Pseudovalence charge density contour plots of the $O_\gamma-RuO_2$-(110) surface cut through the Ru_{cus} atom along the [1̄10] and the [001] directions from DFT calculations (left and middle). On the right side, the surface is cut through the bridging O atom to compare the charge density of O_{br} with that of O-ontop (left side). These plots are defined as the difference between the total valence electron density, as determined by DFT calculations, and a linear superposition of radially symmetric atomic charge densities. Contours of constant charge density are separated by 0.15 eV/Å^3. Electron depletion and accumulation are marked by broken and solid lines. In addition, regions of charge accumulation are darker shadowed than those of charge depletion.

TABLE 4: Dissociative Sticking Coefficient of Oxygen on Ru(0001) and RuO_2(110)

O species	sticking coeff.	ref
initial	0.40	37
Ru(0001)−(2×2)-O	0.40	37
Ru(0001)−(2×)-O	0.04	23
Ru(0001)−(2×2)-3O	0.0003 at 600 K	45
Ru(0001)−(1×1)-O	<0.0001 at 600 K	39
O(on-top)−RuO_2(110)	0.70 at room temp	6

0.3e does not necessarily qualify an electrophilic O species. To elucidate this point, we consider the Ru(0001)−(2×2)-O overlayer. According to our DFT calculations only a small charge transfer of 0.2e takes place from Ru to O, making chemisorbed O a possible candidate for electrophilic oxygen. Now consider the coadsorption of the strongly electropositive Cs species onto the Ru(0001)−(2×2)-O surface at low sample temperatures. Clearly, one would expect that the electrophilic O species is to accumulate electron density from the Cs 6s level. This, however, was not observed, neither in the experiment nor in the DFT calculations.[36]

3.5. Kinetics. Values for the dissociative sticking coefficient of oxygen on Ru(0001) and RuO_2(110) are compiled in Table 4. The initial sticking coefficient of oxygen on Ru(0001) is 0.4 at a sample temperature of 300 K [37] and then drops to below 0.04 for coverages of 0.5 monolayer.[23] Under typical ultrahigh vacuum conditions, the (2 × 1) phase is then also the effective saturation coverage due to the small sticking probability beyond 0.5 monolayer. Excessive oxygen exposure is however able to create (2×2)-3O [38] and (1×1)-O overlayers.[19] In the coverage regime from 0.5 to 1.0 monolayer, the sticking coefficient is only about 3×10^{-4} at 600 K. To accommodate even more oxygen on the Ru(0001)−(1×1)-O, the sample temperature has to be raised to 600−800 K. The dissociative sticking probability on the Ru(0001)−(1×1)-O surface is smaller than 10^{-4} in this temperature range, [6] at room temperature even below 10^{-6}.[39] It is therefore quite surprising that the dissociative sticking probability of oxygen on RuO_2(110) surface is as high as 0.7.[6] A natural explanation may be given by the presence of the molecular precursor state on RuO_2(110). Our DFT calculations revealed a molecular state which bridges two neighboring Ru_{cus} atoms and is bound by 0.8 eV. Hence, the residence time and the mobility of chemisorbed O_2 on RuO_2(110) is quite large at room temperature. This qualifies the chemisorbed O_2 species as a precursor state for the dissociation process, thus rationalizing the high dissociative sticking probability of O_2 over RuO_2(110).

Furthermore, O_γ and/or the molecular species O_δ is mandatory for replenishing the oxygen vacancies of the RuO_2(110) catalyst while the catalytic CO oxidation reaction is in progress. We demonstrated in a previous paper[5] that the CO oxidation over RuO_2(110) under reducing conditions consumes lattice oxygen, presumably the bridging oxygen O_{br}. To maintain a stable RuO_2(110) catalyst under reaction conditions, the loss of lattice oxygen has to be compensated for by the oxygen supply from the gas phase. In fact, this is accomplished by O_2 exposure at 550 K as evidenced by SPALEED investigations.[40] At a sample temperature of 550 K, the LEED intensities of the RuO_2 related reflections decreased markedly during CO exposure (total CO dose: 5 langmuirs); recall that, at a sample temperature of 550 K, CO recombines readily with lattice oxygen to form CO_2. However, only small doses of oxygen (5 langmuirs) at a sample temperature of 550 K were required to repair the defect surface and to restore the original LEED intensity. Most probably, the sequence $O_2(gas) \rightarrow O_{2(\delta)} \rightarrow O_\gamma \rightarrow O_\beta$ is responsible for this effect. An alternative route for restoring a defect-free RuO_2(110) surface is flashing the surface to 700 K. At such a high temperature, oxygen diffusion from deeper layers fills in the CO induced vacancies. The weakly held oxygen O_γ also governs the actual growth of RuO_2(110) on Ru(0001). In a previous STM investigation,[41] we observed that RuO_2(110) grows in large patches, which are separated by large areas of (1×1)-O. Both areas extend over several 10 μm across the surface.[41] Recent PEEM (photoemission electron microscopy) investigations on oxygen-rich Ru(0001) surfaces observed a similar behavior.[42] We interpret the presence of large RuO_2(110) domains as initiated by a low density of RuO_2 nuclei, and once a nucleus has been formed on Ru(0001), it grows rapidly to large domains of RuO_2(110). The weakly held oxygen O_γ may drive this growth mode, since the dissociative sticking coefficient of oxygen on RuO_2(110) is 0.7,[6] while on (1×1)-O the sticking coefficient is smaller than 10^{-4}. The rate-limiting step in the growth of RuO_2(110) is likely to be imposed by the supply of Ru atoms. The thickness of the RuO_2(110) islands was found to be limited to 10−20 Å.[5] This may be rationalized by a small diffusion coefficient of Ru and O atoms through the oxide layer, while diffusion across the oxide layer is high, as also suggested by the growth of large flat oxide islands.

4. Chemical Properties and Outlook

The presence of the weakly bound oxygen O_γ is crucial for the CO oxidation reaction at room temperature.[6] This was recently also verified by Zang and Kisch,[43] who demonstrated that, even under humid (and normal pressure) conditions, CO is readily oxidized to CO_2 at room temperature over large-area RuO_2 films. Obviously, water is not interfering with the CO oxidation reaction, quite unexpected for metal oxides.

Probably more exciting than the total oxidation reaction of CO to CO_2 is the addition of oxygen to unsaturated hydrocarbons. In the epoxidation reaction, an O atom is inserted into the C═C double bond, forming a highly strained and therefore reactive three-member C−O−C ring. To explain the selectivity of this reaction, the concept of electrophilic (i.e. electron accepting, oxygen in a lower valence state) oxygen has been introduced for Ag catalysts.[3,34] As discussed in section 3.4, O_γ

on RuO_2(110) may be regarded as a possible candidate for an "electrophilic" O species. On Ag surfaces, the identification and characterization of this particular oxygen species is severely hampered by the experimental conditions, i.e., excessive oxygen pretreatment, under which this species is stabilized on Ag surfaces. This makes it difficult to eliminate spurious effects due to contamination. O_γ on RuO_2(110), in contrast, might offer the challenging perspective for studying the epoxidation reaction even under ultrahigh vacuum conditions.

We emphasize that the epoxidation reaction differs profoundly from the partial or total oxidation reaction of organic molecules where the C−H bonding is activated by nucleophilic oxygen species, such as the lattice oxygen of RuO_2(110). For a partial dehydrogenation of methanol to formaldehyde, rather the bridging oxygen atoms on RuO_2(110) are considered to be of importance.

5. Conclusion

We characterized the various oxygen species on the RuO_2(110) surface and compared them with adsorbed O layers on Ru(0001) in terms of the local adsorption geometry, vibrational modes, electronic properties, and kinetics. Besides the lattice oxygen (O_β) of RuO_2(110), the chemisorbed molecular oxygen (O_δ) and a weakly held atomic oxygen (O_γ) are stabilized on RuO_2. In this paper, the O_γ species is identified with adsorbed oxygen atoms, which are located in the terminal position above the coordinatively unsaturated Ru sites (Ru_{cus}) on RuO_2(110). The O−Ru stretching modes of O_γ and the bridging oxygen on RuO_2(110) are characterized by vibrational losses at 103 and 69 meV, respectively. The molecular oxygen species (O_δ) adsorbs parallel to the RuO_2(110) surface (chemisorption energy: 0.8 eV), bridging neighboring Ru_{cus} atoms. O_δ on RuO_2(110) may play a crucial role in the dissociation of O_2 over RuO_2(110) and together with (O_γ) also in restoring an O deficient RuO_2(110) surface.

Acknowledgment. We are grateful to Robert Schlögl and Valerii Bukhtiyarov for stimulating discussions. We thank Gerhard Mestl for bringing unpublished results of the terminal O on MoO_3 to our attention.

References and Notes

(1) Ertl, G., Knözinger; H., Weitkamp, J., Eds. *Handbook of Heterogeneous Catalysis*, Vol. 5; Wiley: New York, 1997.

(2) (a) Bao, X.; Barth, J. V.; Lehmpfuhl, G.; Schuster, R.; Uchida, Y.; Schlögl, R. *Surf. Sci*. **1993**, *284*, 14. (b) Bao, X.; Muhler, M.; Pettinger, B.; Schlögl, R.; Ertl, G. *Catal. Lett*. **1993**, *22*, 215. (c) Bao, X.; Muhler, M.; Pettinger, B.; Uchida, Y.; Lehmpfuhl, G.; Schlögl, R. *Catal. Lett*. **1995**, *32*, 171.

(3) (a) Grant, R. B.; Lambert, R. M. *J. Catal*. **1985**, *92*, 364. (b) Bukhtiyarov, V. I.; Kaichev, V. V.; Prosvirin, I. P.; Podgornov, E. A. *Catal. Lett*. **1999**, *57*, 233, and references cited therein.

(4) Over, H. *Prog. Surf. Sci*. **1998**, *58*, 249, and references cited therein.

(5) Over, H.; Kim, Y. D.; Seitsonen, A. P.; Wendt, S.; Lundgren, E.; Schmid, M.; Varga, P.; Morgante, A.; Ertl, G. *Science* **2000**, *287*, 1474.

(6) Böttcher, A.; Niehus, H. *Phys. Rev. B* **1999**, *60*, 14396.

(7) Böttcher, A.; Rogozia, M.; Niehus, H.; Over, H.; Ertl, G. *J. Phys. Chem. B* **1999**, *103*, 6267.

(8) Kim, Y. D.; Seitsonen, A. P.; Over, H. *Surf. Sci*. **2000**, *465*, 1.

(9) Kim, Y. D.; Over, H.; Krabbes, G.; Ertl, G. *Top. Catal*. **2001**, *14*, 95.

(10) Henrich, V. E.; Cox, P. A. *The Surface Science of Metal Oxides*; Cambridge University Press: Cambridge, U.K., 1996.

(11) Over, H.; Bludau, H.; Skottke-Klein, M.; Moritz, W.; Ertl, G. *Phys. Rev. B* **1992**, *46*, 4360.

(12) Moritz, W. *J. Phys. C* **1983**, *17*, 353.

(13) (a) Kleinle, G.; Moritz, W.; Ertl, G. *Surf. Sci*. **1990**, *226*, 119. (b) H. Over, H.; Ketterl, U.; Moritz, W.; Ertl, G. *Phys. Rev. B* **1992**, *46*, 15438. (c) Gierer, M.; Over, H.; Moritz, W. Unpublished material.

(14) Pendry, J. B. *J. Phys. C* **1980**, *13*, 937.

(15) Perdew, J. P.; Burke, K.; Enzerhof, M. *Phys. Rev. Lett*. **1996**, *77*, 3365.

(16) Troullier, N.; Martins, J. L. *Phys. Rev. B* **1993**, *43*, 1991.

(17) Malik, I. J.; Hrbek, J. *J. Vac. Sci. Technol. A* **1992**, *10*, 2565.

(18) Over, H.; Lundgren, E.; Wiklund, M.; Andersen, J. N. Unpublished material.

(19) Kim, Y. D.; Seitsonen, A. P.; Over, H. *Phys. Rev. B.*, in press.

(20) Wurth, W.; Stöhr, J.; Feulner, P.; Pan, X.; Bauchspiess, K. R.; Baba, Y.; Hudel, E.; Rocker, G.; Menzel, D. *Phys. Rev. Lett*. **1990**, *65*, 2426.

(21) Eichler, A.; Hafner, J. *Phys. Rev. Lett*. **1997**, *79*, 4481.

(22) Seitsonen, A. P. Unpublished DFT calculations.

(23) Surnev, L.; Rangelov, G.; Bliznakov, G. *Surf. Sci*. **1983**, *159*, 299.

(24) Stampfl, C.; Kreuzer, H. J.; Payne, S. H.; Pfnür, H.; Scheffler, M. *Phys. Rev. Lett*. **1999**, *83*, 2993.

(25) Stampfl. C.; Schwegmann, S.; Over, H.; Scheffler, M.; Ertl, G. *Phys. Rev. Lett.* **1996**, *77*, 3371.

(26) Zhang, C. J.; Hu, P.; Alavi, A. *J. Chem. Phys.* **2000**, *112*, 10564.

(27) Tokarz-Sobieraj, R.; Hermann, K.; Witko, M.; Blume, A.; Wild, U.; Mestl, G.; Knop-Gericke, A.; Schlögl, R. To be submitted for publication in *Surf. Sci.*

(28) Hermann, K.; Witko, M.; Druzinic, R. *Faraday Discuss*. **1999**, *114*, 53.

(29) (a) Mestl, G.; Ruiz, P.; Delmon, B.; Knözinger, H. *J. Phys. Chem.* **1994**, *89*, 11269. (b) Mestl, G.; Srinivasan, T. K. K. *Catal. Rev.−Sci. Eng*. **1998**, *40*, 451.

(30) He, P.; Jacobi, K. *Phys. Rev. B* **1997**, *55*, 4751.

(31) Kötz, R.; Stucki, S. *J. Electroanal. Chem*. **1984**, *172*, 211.

(32) Chan, H. Y. H.; Takoudis, C. G.; Weaver, M. J. *J. Catal*. **1997**, *172*, 336.

(33) Lin, W. F.; Zei, M. S.; Kim, Y. D.; Over, H.; Ertl, G. *J. Phys. Chem. B* **2000**, *104*, 6040.

(34) van Santen, R. A.; de Groot, C. P. M. *J. Catal*. **1986**, *98*, 364.

(35) van Santen, R. A. In *Handbook of Heterogeneous Catalysis*, Vol. 5; Ertl, G., Knözinger, H., Weitkamp, J., Eds.; Wiley: New York, 1997; p 2244.

(36) Kim, Y. D.; Zhu, Y. J.; Wendt, S.; Seitsonen, A. P.; Schwegmann, S.; Bludau, H.; Over, H.; Morgante, A.; Christmann, K. *Phys. Rev. B* **2000**, *64*, 8455.

(37) Wheeler, M. C.; Seets, D. C.; Mullins, C. B. *J. Chem. Phys*. **1996**, *105*, 1572.

(38) Kostov, K. L.; Gsell, M.; Jacob, P.; Moritz, T.; Widdra, W.; Menzel, D. *Surf. Sci*. **1997**, *394*, L138.

(39) Böttcher, A.; Niehus, H. *J. Chem. Phys*. **1999**, *110*, 3186.

(40) Wendt, S.; Kim, Y. D.; Over, H. Unpublished material.

(41) Over, H.; Lundgren, E.; Schmid, M.; Varga P. Unpublished material.

(42) Böttcher, A.; Conrad, H.; Niehus, H. *Surf. Sci.* **2000**, *452*, 125.

(43) Zang l.; Kisch, H. *Angew. Chem.. Int. Ed. Engl.*. **2000**, *39*, 3921.

(44) Mitchell, W. J.; Wang, Y.; Schick, M.; Weinberg, W. H. *J. Chem. Phys*. **1995**, *102*, 8185.

(45) Jakob, P.; Gsell, M.; Menzel, D. *Phys. Rev. B* **1999**, *59*, 13285.

(46) Jacobi, K. *Landolt Börnstein*, Vol. 24B; Springer: Berlin, 1994; p 66.